Applications of SOLEDGE-2D code to complex SOL configurations and analysis of Mach probe measurements

Hugo Bufferand, Guido Ciraolo, Livia Isoardi, Guillaume Chiavassa, Frédéric Schwander, Eric Serre, Nicolas Fedorczak, Philippe Ghendrih, Patrick Tamain

Applications of SOLEDGE-2D code to complex SOL configurations and analysis of Mach probe measurements

H. Bufferand [a], G. Ciraolo [a,*,1], L. Isoardi [a], G. Chiavassa [a], F. Schwander [a], E. Serre [a], N. Fedorczak [b], Ph. Ghendrih [b], P. Tamain [b]

[a] M2P2, UMR 6181, CNRS Aix-Marseille Université, Ecole Centrale Marseille, Technopole de Cha^teau Gombert, 38 Rue F. Joliot-Curie, 13451 Marseille, France
[b] CEA, IRFM, 13108 St. Paul-Lez-Durance, France

A series of experiments dedicated to the determination of the ballooning nature of the edge and SOL transport has been achieved on Tore Supra [1,2], proposing a quantitative characterization of the radial flux that enters the SOL. The aim of this paper is to back up the interpretation of these probe flow measurements making use of SOLEDGE-2D code. In particular, this fluid code allows one to study density and parallel momentum transport in a 2D geometry including edge and SOL region. Moreover, thanks to an appropriate numerical technique recently proposed [3,4], SOLEDGE-2D code is also able to deal with a complex geometry of plasma facing components including main and secondary limiters.

1. Introduction

A better understanding of the interplay between edge and SOL plasma is a matter of growing concern. Transport properties in this region of transition from closed to open magnetic flux surfaces have been recently investigated by experimental and numerical means in order to determine, for example, the relationship between the strong asymmetries in the SOL parallel flows and the core plasma rotation [5]. Another related and crucial topic for developing future fusion reactors is the possibility of quantitatively predicting and hopefully controlling the power deposition on the plasma facing components. In this context, we analyse a series of experiments performed on Tore Supra, dedicated to the determination of the ballooning nature of the edge and SOL transport [1,2]. Moreover, we will use SOLEDGE-2D code to perform synthetic numerical experiments and study plasma flows in complex SOL geometries.

The paper is organized as follows: in the next section, the experimental results we consider for analysis are presented. Then the SOLEDGE-2D code used for the comparison with measurements is introduced and simulation results for one-limiter SOL are presented. Finally, the last section deals with the influence of a secondary limiter and the comparison with experimental measurements.

* Corresponding author.
E-mail address: guido.ciraolo@l3M.univ-mrs.fr (G. Ciraolo).
[1] Presenting author.

2. Mach probe measurements in the SOL of Tore Supra and estimations of radial flux

The radial flux that enters and propagates into the SOL can be measured by using a reciprocating Mach probe. In Tore Supra, this probe is located at the top of the tokamak (see Fig. 1). It performs radial plunges into the SOL to measure the density and Mach number for a range of radial positions. The coordinates of the measurement points will be noted (r_p, θ_p). The probe curvilinear abscissa along the field line is noted s_{θ_p}. Assuming total pressure conservation along the field line ($\Pi_t = \mathrm{cst}$) [1], it is possible to deduce from local measurements of density (n_p) and Mach number (M_p) the radial source entering the SOL integrated along a field line at radial position r_p. More precisely, it is possible to determine the source entering between the probe and the limiter, see Eq. (2.1): These source terms will be noted $S^A_{r_{1\mathrm{lim}}}$ on the "left" of the probe and $S^B_{r_{1\mathrm{lim}}}$ on the "right" of the probe, see Fig. 1. Note that we name source all the transverse flux of particles into a given field line. Since we do not consider volumetric sources due to neutral ionization, the source term accounts for the cross-field particle transport. The total source is $S^{\mathrm{total}}_{r_{1\mathrm{lim}}} = S^A_{r_{1\mathrm{lim}}} + S^B_{r_{1\mathrm{lim}}}$. Within this framework, the definition of the source $S^A_{r_{1\mathrm{lim}}}$ is

$$S^A_{r_{1\mathrm{lim}}} = \int_0^{s_{\theta_p}} \Gamma_r \mathrm{d}s = \frac{1}{c_\theta} \int_0^{\theta_p} \Gamma_r \mathrm{d}\theta \tag{2.1}$$

Γ_r is the radial flux and for direct comparison with experiment one introduces $\mathrm{d}s = 1/c_\theta \cdot \mathrm{d}\theta$ where one assumes $c_\theta = 1/(qR_0)$ where q is the safety factor and R_0 the tokamak major radius [6]. The formulas used to derivate an estimation of the sources from the probe

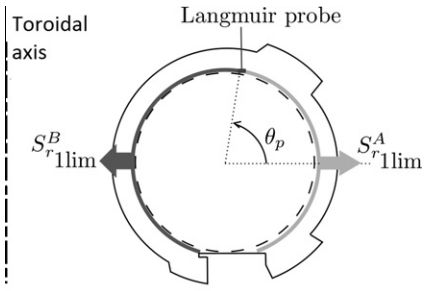

Fig. 1. Poloidal section of Tore Supra. High Field Side (HFS) is on the left, Low Field Side (LFS) is on the right. The Langmuir probe is located on top and the main limiter at the bottom.

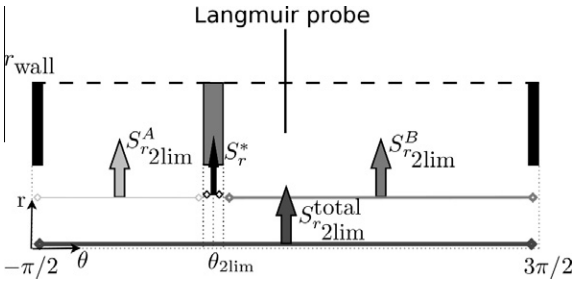

Fig. 2. Two limiters configuration. The main limiter is on the two sides of the periodic box.

measurements are listed in Table 1. In order to have access to the poloidal distribution of the radial source, one would need several Langmuir probes at different poloidal positions. This can be achieved indirectly with a secondary limiter [1]. This is done in Tore Supra with midplane limiters. The configuration of the SOL is represented on Fig. 2 in the (r,θ) plane. On this figure, $\theta_{2\mathrm{lim}}$ is the poloidal position of the secondary limiter. The same notations $S_r^A, S_r^B, S_r^{\mathrm{total}}$ are used to define the sources on each side of the secondary limiter. They will be labeled with the subscript 2lim to distinguish with the previous one-limiter case. The source S_r^* is the effective source entering radially on the top of the limiter, namely without entering the secondary SOL.

Finally, we introduce the peaking-factor $\xi(\theta_0)$ defined as the ratio between the radial source contribution between $\theta = -\pi/2$ and $\theta = \theta_0$ and the total source.

$$\xi(\theta_0) = \frac{\int_{-\pi/2}^{\theta_0} \Gamma_r \mathrm{d}\theta}{\int_{-\pi/2}^{3\pi/2} \Gamma_r \mathrm{d}\theta} \tag{2.2}$$

This function is characteristic of the spatial location of the radial source. For instance, if the source is homogeneous, one should find the linear expression $\xi(\theta) = (\theta + \pi/2)/(2\pi)$. Conversely if all the source is located at the position θ_s, one finds a step function for ξ with a transition from 0 to 1 at $\theta = \theta_s$. The experimental data for ξ obtained on Tore Supra can be fitted with various profiles as displayed on Fig. 3a.

In a simplified approach one can describe the radial flux Γ_r in terms of an effective diffusion. The radial flux is then expressed as the product of a diffusion coefficient $D(\theta)$ times the radial gradient of plasma density. Assuming constant radial density gradients, this poloidal mapping of the radial flux can then be seen as a mapping of an effective diffusivity.

$$\xi(\theta_0) = \frac{\int_{-\pi/2}^{\theta_0} \Gamma_r \mathrm{d}\theta}{\int_{-\pi/2}^{3\pi/2} \Gamma_r \mathrm{d}\theta} \approx \frac{\int_{-\pi/2}^{\theta_0} D(\theta) \mathrm{d}\theta}{\int_{-\pi/2}^{3\pi/2} D(\theta) \mathrm{d}\theta} \tag{2.3}$$

As a first remark, we observe that the slope of the peaking function $\xi(\theta)$ is determined by the local value of the diffusion coefficient $D(\theta)$. In that perspective, two diffusivity profiles, D1 and D2, are used to fit the experimental data, Fig. 3, corresponding to "weakly" and "strongly" ballooned cross-field transport respectively. The minimum diffusivity is set at $D_{\mathrm{min}} = 0.31\ \mathrm{m^2\ s^{-1}}$ for both cases.

These diffusivity profiles are used as input data in the 2D fluid code SOLEDGE-2D [4] to simulate the experiments. While the above analysis is based on constant pressure in the parallel direction, the simulations performed in this paper allows us to introduce viscosity, and thus departure from constant pressure.

Table 1
On the center are the source definitions, on the right are the formulae used in the Langmuir probe data processing.

Notation	Source definition	Estimation using iso-Π_t assumption
$S^{\mathrm{total}}_{r_{1\mathrm{lim}}}$	$1/c_\theta \int_{-\pi/2}^{3\pi/2} \Gamma_r \mathrm{d}\theta$	$q(r_0) \int_{r_0}^{r_{\mathrm{wall}}} \frac{n_p c_s (1+M_p^2)}{q} \mathrm{d}r$
$S^A_{r_{1\mathrm{lim}}}$	$1/c_\theta \int_{-\pi/2}^{\theta_p} \Gamma_r \mathrm{d}\theta$	$q(r_0) \int_{r_0}^{r_{\mathrm{wall}}} \frac{n_p c_s (1+M_p)^2}{2q} \mathrm{d}r$
$S^B_{r_{1\mathrm{lim}}}$	$1/c_\theta \int_{\theta_p}^{3\pi/2} \Gamma_r \mathrm{d}\theta$	$q(r_0) \int_{r_0}^{r_{\mathrm{wall}}} \frac{n_p c_s (1-M_p)^2}{2q} \mathrm{d}r$

3. SOLEDGE-2D code transport equations and penalization technique for limiter modeling

SOLEDGE-2D is a fluid code that focuses on edge and Scrape-Off Layer plasma simulation. In its 2D version it solves fluids equations for density, parallel momentum, ion temperature and electron temperature. The "light" version used for this paper just focuses on density and parallel momentum $\Gamma_\parallel$. The domain considered is the entire SOL and the edge plasma. Assuming toroidal symmetry, the geometrical domain is completely described by the radial coordinate r and the poloidal one θ. The equations are solved in slab approximation (small radial domain Δr with respect to plasma radius a). The turbulent radial transport of density and momentum are simulated with "effective" diffusivities and the plasma is assumed isothermal. This is consistent with the high SOL temperature of limiter plasmas leading to the so-called sheath limited regime. In this version of SOLEDGE-2D one assumes that the interaction with neutrals is small, hence that the radial extent of the domain is small compared to the neutral ionization mean free path. Although this assumption can be correct for limiter plasmas, it will be alleviated in future works. The system solved is given by Eq. (3.1).

$$\begin{cases} \partial_t n + \frac{1}{R_0 q(r)} \partial_\theta \Gamma_\parallel = D \partial_r^2 n \\ \partial_t \Gamma_\parallel + \frac{1}{R_0 q(r)} \partial_\theta \left(\frac{\Gamma_\parallel^2}{n} + (p_e + p_i)/m_i \right) = v \partial_r^2 \Gamma_\parallel \end{cases} \tag{3.1}$$

where D and v are diffusion coefficients that can be adjusted to account for the radial transport mechanisms. This system is written with dimensionless variables and a penalization term is added to force the solution to a selected value in chosen regions of the domain. The dimensionless system solved in SOLEDGE-2D is given by

$$\begin{cases} \partial_t N + \frac{1}{q} \partial_\theta \Gamma + \frac{\chi}{\eta} N = \frac{A}{\mathrm{Pe}} \partial_r^2 N \\ \partial_t \Gamma + \frac{1}{q}(1-\chi) \partial_\theta \left(\frac{\Gamma^2}{N} + N \right) + \frac{\chi}{\eta}(\Gamma - \Gamma_0) = \frac{A\,\mathrm{Sc}}{\mathrm{Pe}} \partial_r^2 \Gamma \end{cases} \tag{3.2}$$

where $\Gamma = \Gamma_\parallel/(n_0 c_s)$ and $N = n/n_0$. c_s is the sound speed, the characteristic time is the transit time at sound speed in the parallel direction $\tau = L_\parallel/c_s$. The characteristic length in the parallel direction is $L_\parallel = 2\pi R_0$. In the simulation we consider in this paper, we have chosen $2\ \pi R_0 = 16$ m and the sound speed is calculated with $T_e + T_i = 65$ eV which gives c_s equal to $7.94 \cdot 10^4$ m/s. The safety factor q varies radially from 3.8 to 6.4. The connection length is then of

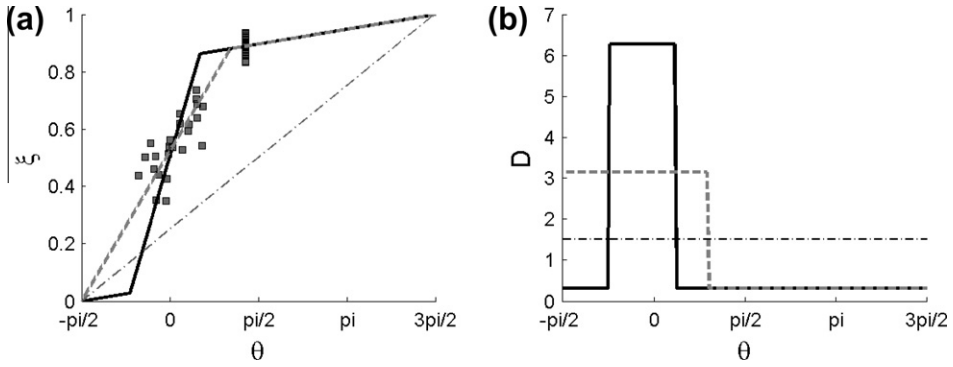

Fig. 3. (a) Experimental data (symbols) from Fedorczak et al. (in press) [2] representing the peaking function $\xi(\theta)$ and linear fits. Homogeneous diffusivity case is represented for comparison (dash–dot line). (b) Corresponding diffusivity profiles: D1, weakly ballooned (grey-dash) – D2, strong ballooned (black-solid) – homogeneous (dash–dot).

the order of 80 m. The SOL density decay length is chosen to be about 2 cm when diffusivity is minimum which gives as mentioned before a minimum diffusivity $D_{\min} = 0.31\ \mathrm{m^2\ s^{-1}}$. The size of the domain simulated in the perpendicular direction is chosen to be $L_r = 30$ cm. The dimensionless density gradient is set to *1* at the edge boundary, hence, the characteristic density n_0 is linked with the flux entering from the core region by the relation $\Gamma_r^{\mathrm{in}}(\theta) = D(\theta)\cdot n_0/L_r$. In Eq. (3.2), $A = L_\parallel/L_r$, is the aspect ratio ($A = 50$), Pe is the Peclet number defined as $\mathrm{Pe} = L_r c_s/D$ and $\mathrm{Sc} = \nu/D$ is the Schmidt number. Given the poloidal diffusivity profiles plotted on Fig. 3, the Peclet number is found to vary between 4000 and 80000.

The penalization technique allows one to add an obstacle of any shape in the domain. The obstacle is defined through a mask function χ equals to one in the region where the obstacle is located and zero elsewhere. In this case, the mask function represents a toroidal limiter with poloidal extent $\pi/15$. The penalization technique consists in forcing the solution to a selected value in a region of the domain. In the case of a limiter immersed in a tokamak plasma, for example, the density is forced to be zero in the limiter region. The momentum equation is also penalized, as shown in Eq. (3.2). In the region where the mask function is equal to zero, one recovers the transport equations for density and momentum as described by the Eq. (3.1), [3].

On Fig. 4, one has plotted the 2D contours of Mach number for the diffusivity profile D1. One notices that the stagnation point is located on the outer midplane where the radial transport is maximum. Under the assumption of conservation of pressure, the stagnation point is located where the peaking factor ξ is equal to 1/2. The values of Mach number on the limiter are in good agreement with Bohm conditions.

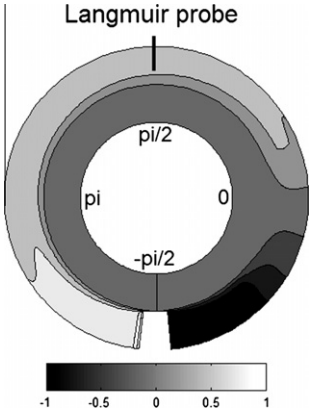

Fig. 4. Mach number contour plot. Simulation results with diffusivity profile D2.

4. Synthetic Langmuir probe measurements

In order to validate the approximation made in the experiment, a synthetic Langmuir probe experience is carried out in the simulated field of density and velocity at the poloidal position $\theta = \pi/2$. Following the experimental data processing, see Table 1, one obtains the radial sources. Then, this *synthetic* source is compared to the *actual* source values computed with the full simulation data. With the diffusivity profile labeled D2, the probe gives a *synthetic* peaking-factor of 0.813 on the LFS whereas the *actual* value is 0.799. With the diffusivity profile D1, the *synthetic* value of ξ is 0.836 whereas the *actual* value is 0.807. In both case, the error is of a few percents which is well below the experimental error bars. More precisely, one notices that the total pressure exhibits a parallel relative variations of 15% at the LCFS where the momemtum gradients are the strongest. However, the radial integration leads to a compensation of this pressure variation effect. This property is related to momentum conservation so that the assumption leading to expressions of Table 1 weakly depart from simulation data.

5. Simulation of 2-limiters SOL

A secondary limiter is introduced in the domain using the penalization technique. This limiter is also $\pi/15$ wide in the poloidal direction and its position can be adjusted from $\theta = -\pi/5$ to $\theta = \pi/5$ to reproduce the experiment carried out in Tore Supra. In the present analysis the two limiters have the same radial extent, see Fig. 5.

The experiment consists in measuring the radial flux on one side of this secondary limiter and compare it with the total flux entering the SOL. In the experimental data processing, we assume that the secondary limiter does not change the value of the radial source entering at the LCFS. Hence we consider that the measurement of the total source made without the secondary limiter is such that $S_{r_{1\mathrm{lim}}}^{\mathrm{total}} \approx S_{r_{2\mathrm{lim}}}^{\mathrm{total}}$. Consistent with $S_{r_{2\mathrm{lim}}}^{*} \approx 0$ giving $S_r^{\mathrm{total}} = S_r^A + S_r^B + S_r^* \approx S_r^A + S_r^B$, the ξ function can thus be evaluated with Eq. (5.1).

$$\xi^{\mathrm{actual}}(\theta_{2\mathrm{lim}}) = \frac{S_{r_{2\mathrm{lim}}}^A}{S_{r_{2\mathrm{lim}}}^A + S_{r_{2\mathrm{lim}}}^B} = 1 - \frac{S_{r_{2\mathrm{lim}}}^B}{S_{r_{2\mathrm{lim}}}^A + S_{r_{2\mathrm{lim}}}^B} \tag{5.1}$$

$$\begin{aligned}\xi^{\mathrm{synthetic}}(\theta_{2\mathrm{lim}}) &= 1 - \frac{S_{r_{2\mathrm{lim}}}^B}{S_{r_{1\mathrm{lim}}}^{\mathrm{total}}} \approx 1 - \frac{S_{r_{2\mathrm{lim}}}^B}{S_{r_{2\mathrm{lim}}}^A + S_{r_{2\mathrm{lim}}}^B + S_{r_{2\mathrm{lim}}}^*} \\ &\approx \xi^{\mathrm{actual}}(\theta_{2\mathrm{lim}}) + \frac{S_{r_{2\mathrm{lim}}}^B \cdot S_{r_{2\mathrm{lim}}}^*}{\left(S_{r_{2\mathrm{lim}}}^A + S_{r_{2\mathrm{lim}}}^B\right)^2}\end{aligned} \tag{5.2}$$

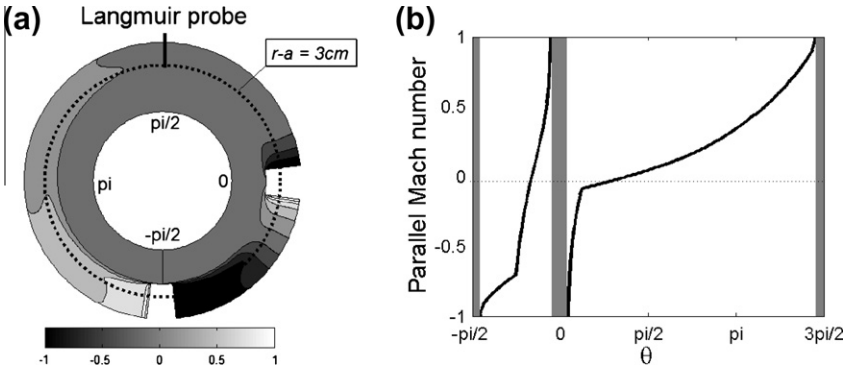

Fig. 5. (a) Mach number contour plot. Simulation results for diffusivity profile D2. The main limiter is at the bottom. The secondary limiter is on the LFS (right, $\theta_{2\mathrm{lim}} = 0$). (b) Mach number poloidal profile for $r = a + 3$ cm.

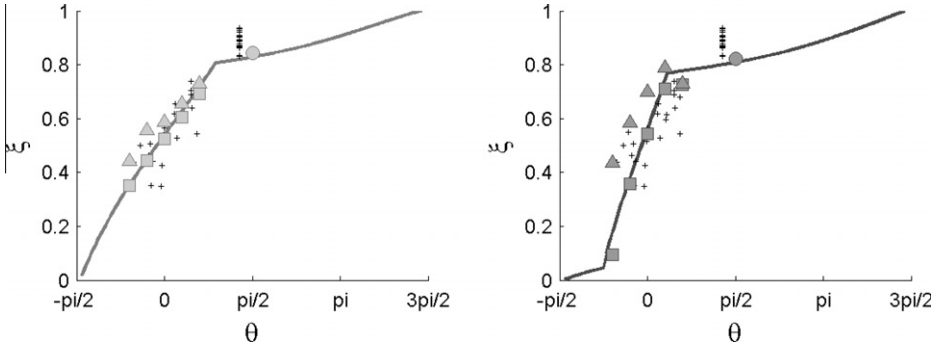

Fig. 6. Weakly ballooned diffusivity case D1 (Left) and strong ballooned diffusivity case D2 (Right) – Lines: ξ functions computed in unperturbed one-limiter SOL. Symbols: Circle (synthetic): Langmuir probe measurements in simple SOL configuration; squares (actual): estimation of ξ in the two limiters configuration; triangles (synthetic) and crosses (experimental): estimation of ξ in the two limiters configuration.

The effective source $S^A_{r_{2\mathrm{lim}}}$ and $S^B_{r_{2\mathrm{lim}}}$ are calculated as well as $\xi = S^A_{r_{2\mathrm{lim}}}/(S^A_{r_{2\mathrm{lim}}} + S^B_{r_{2\mathrm{lim}}})$ for five secondary limiter positions in the vicinity of the midplane. The data representing the *actual* values of the peaking factor at $\theta = \theta_{2\mathrm{lim}}$ are plotted on Fig. 6 with full squares. On the same Figure are plotted with triangles the *synthetic* values. One can notice that the experimental data processing leads one to overestimate the peaking factor by neglecting the source that enters radially into the limiter S^*_r, see Eq. (5.2). This problem would be overcome by using two Langmuir probes, one measuring $S^A_{r_{2\mathrm{lim}}}$ and the other measuring $S^B_{r_{2\mathrm{lim}}}$. Finally, on Fig. 6 one also plots the peaking factor ξ calculated without the secondary limiter (solid line). One can notice that there is a weak departure between the single and two limiters cases. Consequently, the presence of a secondary limiter does not appear to modify drastically the localization of the sources.

6. Conclusions

Complex SOL geometries with two limiters have been simulated in the fluid code SOLEDGE-2D by using penalization technique. Synthetic Langmuir probe experiments have been performed with different ballooned cross-field transport properties. These simulation results have been compared with experimental measurements performed on Tore Supra and show a good agreement. Besides, if the experimental data processing assumes total pressure conservation along the field line, the simulations show that pressure variations effect is weak and only induces an error of a few percents on the peaking factor value. In that sense, it backs up the experimental analysis. The experimental data processing also neglects the particle flux entering radially into the limiter. In Tore Supra's experimental setup, neglecting this flux results in a systematic overestimation of the peaking factor. The simulations make possible to evaluate this up-shift and thus give a better estimation of the radial transport ballooning.

Acknowledgements

This work is supported by the ANR project ESPOIR ANR-09-BLAN-0035-01 and by the European Communities under the contract of Association between EURATOM and CEA, was carried out within the framework of the European Fusion Development Agreement. The views and opinions expressed herein do not necessarily reflect those of the European Commission.

References

[1] J.P. Gunn et al., J. Nucl. Mater. 363–365 (2007) 484–490.
[2] N. Fedorczak et al., J. Nucl. Mater. 415 (2011) S467–S470.
[3] L. Isoardi et al., J. Comp. Phys. 229 (2010) 2220–2235.
[4] L. Isoardi et al., J. Nucl. Mater. 390-391 (2009) 388.
[5] B. Labombard et al., Nucl. Fusion 44 (2004) 1047.
[6] G. Dif-Pradalier et al., The mistral base case to validate kinetic and fluid turbulence transport codes of the edge and sol plasmas, J. Nucl. Mater., in press.